

Resonant X-Ray Diffraction Study of Strongly Spin-Orbit-Coupled Mott Insulator CaIrO_3

Kenya Ohgushi,^{1,2} Jun-ichi Yamaura,¹ Hiroyuki Ohsumi,³ Kuniyoshi Sugimoto,⁴ Soshi Takeshita,³ Akihisa Tokuda,⁵ Hidenori Takagi,^{2,6,7} Masaki Takata,^{3,4} and Taka-hisa Arima^{2,3,8}

¹*Institute for Solid State Physics, University of Tokyo, Kashiwa, Chiba 277-8581, Japan*

²*JST, TRIP, Chiyoda, Tokyo 102-0075, Japan*

³*RIKEN SPring-8 Center, Sayo, Hyogo 679-8148, Japan*

⁴*Japan Synchrotron Radiation Research Institute, SPring-8, Sayo, Hyogo 679-5198, Japan*

⁵*Department of Physics, Kwansei Gakuin University, Sanda, Hyogo 669-1337, Japan*

⁶*Department of Advanced Materials Science, University of Tokyo, Kashiwa, Chiba 277-8561, Japan*

⁷*Advanced Science Institute, RIKEN, Wako, Saitama 351-0198, Japan*

⁸*Institute of Multidisciplinary Research for Advanced Materials, Tohoku University, Sendai, Miyagi 980-8577, Japan*

(Dated: August 24, 2011)

We performed resonant x-ray diffraction experiments at the L absorption edges for the post-perovskite-type compound CaIrO_3 with $(t_{2g})^5$ electronic configuration. By observing the magnetic signals, we could clearly see that the magnetic structure was a striped order with an antiferromagnetic moment along the c -axis and that the wavefunction of a t_{2g} hole is strongly spin-orbit entangled, the $J_{\text{eff}} = 1/2$ state. The observed spin arrangement is consistent with theoretical work predicting a unique superexchange interaction in the $J_{\text{eff}} = 1/2$ state and points to the universal importance of the spin-orbit coupling in Ir oxides, irrespective of the local coordination and lattice topology. We also propose that the non-magnetic resonant scattering is a powerful tool for unraveling an orbital state even in a metallic iridate.

PACS numbers: 75.25.-j, 75.25.Dk, 78.70.Ck, 75.50.Ee

There is a new trend toward exploring Mott physics in a system with a strong spin-orbit interaction [1–5]. Theoretical calculations on the Hubbard model revealed that the spin-orbit interaction drives a transition from a correlated metal to an insulator [3–5]. This novel Mott insulating state is actually realized in a layered perovskite Sr_2IrO_4 , including Ir^{4+} ions with a $(t_{2g})^5$ electronic configuration [1, 2]. In this compound, one hole among t_{2g} manifolds takes a complex wavefunction with the spin and orbital magnetic moments of $1/3$ and $2/3 \mu_B$, respectively. This so-called $J_{\text{eff}} = 1/2$ state is achieved by the superiority of the spin-orbit interaction over the tetragonal crystal field around the $5d$ transition element.

The superexchange interaction between two Ir^{4+} ions in the $J_{\text{eff}} = 1/2$ state is theoretically shown to be unique [6]. Whereas an antiferromagnetic Heisenberg interaction $J_1 \mathbf{S}_i \cdot \mathbf{S}_j$ (\mathbf{S}_j being the spin at the j -th Ir site) is dominant in a corner-shared IrO_6 bond (the Ir–O–Ir bond angle being 180°), it completely vanishes in the edge-shared IrO_6 bond (the Ir–O–Ir bond angle being 90°) owing to an interference effect. Instead, the magnetic interaction of the edge-shared bonds becomes a highly anisotropic and ferromagnetic one, $-J_2 \mathbf{S}_i^z \mathbf{S}_j^z$, where the z direction is perpendicular to the plane expanded by the two Ir atoms and two O atoms responsible for the edge-shared bond [Fig. 1(a)]. This interaction, which is called the quantum compass model, is unique in the sense that the spin anisotropy is produced by the perturbation effect of the Hund’s coupling (not the spin-orbit interaction). To test the validity of this theory, it

is necessary to elucidate the magnetic structure of an Ir oxide with an edge-sharing network.

CaIrO_3 forms the post-perovskite structure shown in Fig. 1 (a). It is composed of edge-shared (corner-shared) IrO_6 octahedra along the a -(c)-axis, where each octahedron is compressed along the corner-shared O direction (the z direction) with a bond length ratio of 0.97 [7]. This structure is in stark contrast to Sr_2IrO_4 , where elongated IrO_6 octahedra with the bond length ratio 1.04 are connected solely by sharing corners. Hence, CaIrO_3 is an ideal platform for investigating the universal role of spin-orbit coupling in Ir oxides. The compound shows a Mott insulating behavior characterized by the charge gap ~ 0.17 eV and undergoes a transition to a possibly canted antiferromagnetic state at 115 K ($= T_N$) [8]. A deviation from the Curie-Weiss law above T_N as well as large coercive fields below T_N suggest an emergence of the spin-orbit interaction.

In this Letter, we investigated the magnetic and orbital structure of CaIrO_3 by using the resonant x-ray diffraction [9] at the L absorption edges. This technique is particularly powerful in compounds with $5d$ transition metals because the wavelength of the x-ray beam is comparable to the lattice parameters [2, 10–12] and the scattering amplitude is enhanced due to a dipole-allowed nature. We also note that neutron scattering measurements are not applicable to the present system with a strong neutron-absorbing element Ir. We clarify that the magnetic structure of CaIrO_3 is a striped-type one and that the $J_{\text{eff}} = 1/2$ orbital state is realized also in a com-

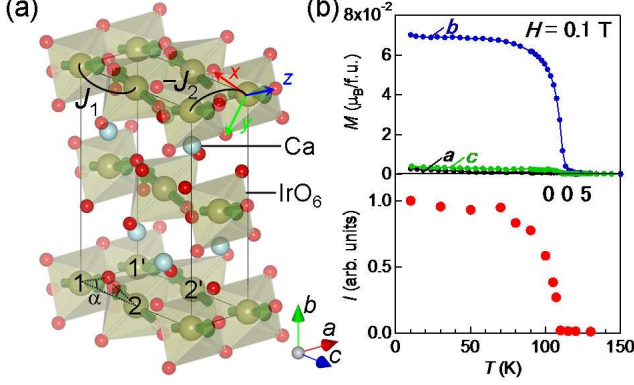


FIG. 1: (Color online) (a) Crystal structure of the post-perovskite CaIrO_3 . The solid lines indicate the conventional unit cell, which is twice as large as the primitive unit cell. The magnetic interaction, as well as the magnetic structure determined in this study, are also shown. (b) Temperature (T) dependence of the magnetization (M) at the magnetic field (H) of 0.1 T [13] (upper), and the intensity (I) of the 0 0 5 reflection at $\psi = 0$ (lower).

pressed octahedral coordination. We then compare these results with theoretical predictions.

Single crystalline CaIrO_3 was grown by the flux method. CaCO_3 , IrO_2 , and CaCl_2 with a molar ratio of 1:1:16 was slowly cooled from 1200 °C to 1000 °C for 240 h. Resonant x-ray diffraction measurements were performed at the beamline BL19LXU at SPring-8 [13, 14]. An incident beam was monochromated by a pair of Si (1 1 1) crystals and irradiated on the (0 0 1) surface of the sample, which was mounted in a ^4He closed-cycle refrigerator installed on a four-circle diffractometer with a vertical scattering plane geometry. The intensities of incident and scattered beams were detected by an ionization chamber and a Si PIN photodiode, respectively. The polarization of the incident beam was perpendicular to the scattering plane (σ) and that of the scattered beam was analyzed by using the 0 0 8 reflection of pyrolytic graphite. The azimuthal angle ψ is defined as $\psi = 0^\circ$ when $\sigma \parallel a$. We also performed similar experiments at the beamline BL02B1 at SPring-8, where we use an imaging plate as a detector [15].

Figure 2 displays the absorption spectra obtained by fluorescence measurements at room temperature (T) as well as the energy dependence of the scattered intensity of the 0 0 5 reflection at $T = 10$ K. At $\psi = 0^\circ$ [Fig. 2(b)], we can observe a strong resonance peak at the L_3 edge ~ 11.2 keV; the intensity is about 0.015 % of the fundamental 0 0 4 reflection. There are fine structures denoted by A and B with an integrated intensity ratio of 1:0.20, which origin will be addressed below. The space group of CaIrO_3 is $Cmcm$ orthorhombic symmetry, where 0 0

$2n+1$ reflections are forbidden according to the c -glide reflection. The polarization analysis indicates the π' character of the scattered beam $I_{\sigma-\sigma'}/I_{\sigma-\pi'} = 3\%$ [inset of Fig. 2(b)], which also rules out the Thomson scattering as the origin. The T variation of the integrated intensity well follows that of the weak ferromagnetic moment [Fig. 1(b)]. Considering also that the anisotropic tensor of susceptibility (ATS) scattering is prohibited in this geometry as discussed later, we conclude that the observed reflection originates from a commensurate antiferromagnetic order. Importantly, the 0 0 5 reflection cannot be detected within an experimental accuracy at the L_2 edge ~ 12.82 keV, $I_{L_2}/I_{L_3} < 0.3\%$. At the L_3 edge, we also observed magnetic reflections at 0 0 l with $l = 1, 3, 7$, and 9.

The observed magnetic reflections at 0 0 $2n+1$ are well accounted for by considering an antiparallel arrangement of two Ir spins [labeled 1 and 2 in Fig. 1(a)] in a primitive unit cell. In principle, one can also determine the spin direction experimentally by the ψ dependence of the magnetic signal: $I_{\text{mag}} \propto \sin^2 \psi$, $\cos^2 \psi$, and 1 for the spin direction along the a , b , and c axes, respectively [16]. However, the needle-like crystal morphology along the a axis prevents us from performing such an analysis. We therefore employed the representation analysis, the results of which are summarized in Table I. We note that the crystallographic space group for the magnetic phase below T_N has been revealed to be $Cmcm$ by oscillation photographs obtained at BL02B1. Considering the parasitic ferromagnetism along the b -axis [Fig. 1(b)] together with the second order nature of the magnetic transition, we conclude that the Γ_{3g} representation with the antiferromagnetic moments along the c -axis is realized. The obtained magnetic structure is schematically drawn in Fig. 1(a). It is a stripe-type order with a parallel alignment along the a -axis and an antiparallel alignment along the c -axis. This markedly contrasts with the checkerboard spin arrangement on the IrO_2 plane in Sr_2IrO_4 [2].

We move to the wavefunction of a t_{2g} hole. When the tetragonal crystal field Δ (> 0 for the compressed octahedron) and the spin-orbit coupling ζ are present, the sixfold degenerated t_{2g} orbitals are split into three dou-

TABLE I: The magnetic structures of the irreducible representations (Γ_i) for the $Cmcm$ space group. M denotes the magnetic point group, where $\bar{1}$ stands for the time-reversal operation. a , b , and c represent the spin directions. AF and F denote the antiferromagnetic and ferromagnetic arrangement of spins at two Ir sites in a unit cell.

| Γ_i | M | generators | a | b | c |
|---------------|-------------------------|---------------------|-----|-----|-----|
| Γ_{1g} | mmm | $2_x, 2_y, \bar{1}$ | AF | . | . |
| Γ_{2g} | $m\bar{m}\bar{m}$ | $2_x, 2_y, \bar{1}$ | F | . | . |
| Γ_{3g} | $\bar{m}\bar{m}\bar{m}$ | $2_x, 2_y, \bar{1}$ | . | F | AF |
| Γ_{4g} | $\bar{m}\bar{m}\bar{m}$ | $2_x, 2_y, \bar{1}$ | . | AF | F |

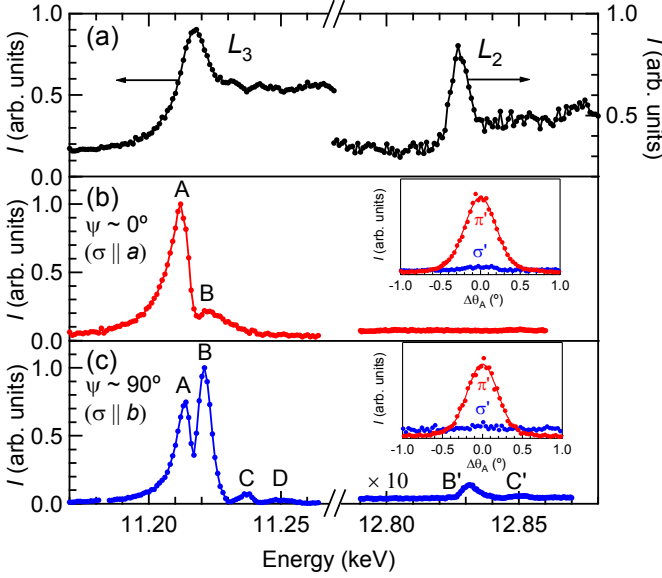


FIG. 2: (Color online) (a) X-ray absorption spectra near the Ir L edge for CaIrO₃. (b) The energy dependence of the magnetic scattering intensity (I) of the 0 0 5 reflection at $T = 10$ K and $\psi = 0^\circ$. The inset shows the polarization analysis of the scattered light at the L_3 edge, where $\Delta\theta_A$ represents the analyzer angle. (c) Same data as (b) except for $\psi = 90^\circ$. The ATS scattering is dominant in this geometry. Note that the data at the L_2 edge is magnified by 10 for clarity.

bly degenerated bands. At the ground state, one hole occupies one of the highest energy orbitals $|\varphi, \pm\rangle = \frac{1}{\sqrt{A^2+2}}(A|xy, \pm\rangle \pm |yz, \mp\rangle + i|zx, \mp\rangle)$, where $A = \frac{-\zeta - 6\Delta + \sqrt{3}\sqrt{3\zeta^2 + 4\zeta\Delta + 12\Delta^2}}{2\zeta}$ quantifies the role of the tetragonal crystal field: $A = 0$ when $\Delta/\zeta = \infty$ and $A = 1$ when $\Delta/\zeta = 0$; the latter corresponds to the $J_{\text{eff}} = 1/2$ state. There has been a simple argument that the orbital character can be determined by the edge dependence of the magnetic scattering intensity [2]. We here discuss this issue in more detail on the basis of CaIrO₃ [13].

When one electron is virtually excited from the $2p$ orbitals in a resonant process, the t_{2g} bands are fully occupied; this simplicity enables us to calculate the atomic scattering tensor straightforwardly. By combining contributions of two Ir sites in a striped-ordered state, we obtain the tensor structure amplitude \hat{F} for the 0 0 $2n + 1$ reflection. Nonzero components in \hat{F} are $F_{ab} = -F_{ba} \equiv iF_{\text{mag}}$ and $F_{bc} = F_{cb} \equiv F_{\text{ATS}}$ [17]. The F_{mag} term changes its sign by applying the time-reversal operation, and represents the magnetic scattering. The F_{ATS} term corresponds to the ATS scattering. The local principal axes towards the corner-shared O, z , of two Ir sites in a primitive unit cell are alternately tilted by an angle $\pm\alpha$ ($\sim 23^\circ$) from the c -axis [Fig. 1(a)]. This difference in the local anisotropy revives 0 0 $2n + 1$ reflections, which are pronounced in a resonant

condition. The scattering intensity shows the polarization and azimuthal dependence as follows: $I_{\sigma-\sigma'} = 0$ and $I_{\sigma-\pi'} = |\cos\theta \sin\psi F_{\text{ATS}} + i \sin\theta F_{\text{mag}}|^2$, where θ is the Bragg angle. The scattering intensity also shows a large difference between at the L_2 and L_3 edges. We can quantitatively estimate this by referring to calculated results: $F_{\text{mag}} = \pm(\cos\alpha/3)f(A^2 - 2A - 2)/(A^2 + 2)$ and $F_{\text{ATS}} = -(\sin 2\alpha/3)f(A^2 + A - 2)/(A^2 + 2)$ for the L_3 edge; and $F_{\text{mag}} = \mp(\cos\alpha/3)f(A - 1)^2/(A^2 + 2)$ and $F_{\text{ATS}} = -(\sin 2\alpha/6)f(A - 1)^2/(A^2 + 2)$ for the L_2 edge. The intensity ratio of the L_2 to L_3 edges are plotted in Fig. 3. One can see that both the magnetic and ATS scattering intensity ratio steeply decrease with approaching to the $J_{\text{eff}} = 1/2$ state ($A = 1$) and that particularly the ATS scattering ratio with a larger value is more useful to determine the orbital character in a large A region than the magnetic scattering ratio.

We now focus on the spectra at $\psi = 90^\circ$ [Fig. 2(c)], where the ATS scattering becomes largest. The ψ -independent magnetic scattering is overlapping; however, we can conclude that the ATS scattering is dominant at $\psi = 90^\circ$, $I_{\text{ATS}}/I_{\text{mag}} \sim 30$ at the L_3 edge, by comparing the intensity at $\psi = 0$ and 90° . We confirmed a π' character of the scattered beam $I_{\sigma-\sigma'}/I_{\sigma-\pi'} = 3.9\%$ [inset of Fig. 2(c)].

At the L_3 edge, we can discern four fine structures centered at 11.214, 11.221, 11.237, and 11.249 keV with an integrated intensity ratio of 1:0.95:0.06:0.04. The first and second peaks, the energies of which coincide with inflection points of the absorption spectrum, are also observed at $\psi = 0^\circ$ and are ascribed to the virtual excitation from the $2p$ $J = 3/2$ orbitals to the t_{2g} and e_g orbitals, respectively (inset of Fig. 3). The energy difference of these two peaks corresponds to the crystal field splitting due to the octahedral crystal field, which is estimated to be $10Dq = 7$ eV. This value is much larger than typical values in the $3d$ and $4d$ transition metal oxides, e.g. $10Dq = 4$ eV in Ca₂RuO₄ [18]. This can be interpreted as the strong covalency effect in a $5d$ transition metal enlarging the band splitting. The higher energy structures denoted by C and D are likely related to the $6s$ and $6p$ bands.

At the L_2 edge, as in the case of $\psi = 0^\circ$, we could not observe any signal at the energy related to t_{2g} orbitals as an intermediate state. We note that a peak structure centered at 12.832 keV corresponds to an inflection point of the absorption spectrum at the *higher* energy side; hence, the intermediate state is e_g orbitals. The intensity ratio at the t_{2g} related energy is $I_{L_2}/I_{L_3} < 0.05\%$. Comparing this observation with calculated results shown in Fig. 3 imposes a restriction of $A > 0.87$. On the other hands, the finite ATS signal at the L_3 edge indicates $A < 1$. We thus conclude that a t_{2g} hole has a slightly modified $J_{\text{eff}} = 1/2$ state. We here point out that the ATS scattering intensity is a quite sensitive probe of the wave function. It should be interesting to apply this probe to

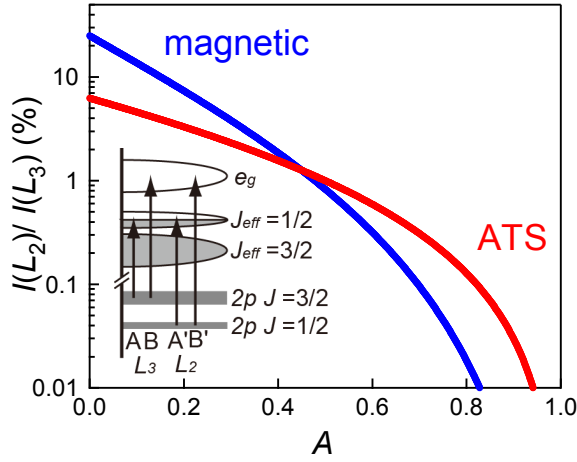


FIG. 3: (Color online) The calculated intensity ratio in the magnetic and ATS scattering of the L_2 to L_3 edges as a function of the A coefficient. The $A = 1$ corresponds to the $J_{\text{eff}} = 1/2$ state. Note that the ordinate is scaled logarithmically. The inset shows the energy scheme of the virtual excitations in resonant processes.

metallic iridates with no magnetic order [8, 19, 20], where various exotic quantum states are anticipated [4, 21].

Our result that the $J_{\text{eff}} = 1/2$ state is realized in CaIrO_3 enables us to argue the magnetic structure in the framework of the theory by Jackeli and Khaliullin unambiguously [6]. We recall that the theory predicts an antiferromagnetic (ferromagnetic) interaction through the corner-(edge)-shared bonds, being consistent with our spin arrangements. Moreover, the weak ferromagnetism along the b -axis can be successfully explained by the theory. There are two mechanisms which induce the spin canting. One is that the anisotropic axis z in the quantum compass model is distinguishable between the $\text{Ir}(1)$ – $\text{Ir}(1')$ and $\text{Ir}(2)$ – $\text{Ir}(2')$ bonds [Fig. 1(a)]. Another is the Dzyaloshinskii–Moriya (D–M) interaction at the $\text{Ir}(1)$ – $\text{Ir}(2)$ bond with the D–M vector $\mathbf{D}_{1,2} = (D, 0, 0)$ (the site symmetry at the midpoint of the bond being $m2m$). A mean field treatment of the Hamiltonian including J_1 - and J_2 -terms, and the D–M interaction gives the most stable spin arrangement to be the experimentally observed stripe-type order with the spin canted angle of α . On the other hands, when we assume the antiferromagnetic magnetic moment of $1 \mu_B/\text{Ir}$, which is the expected value for the completely localized $J_{\text{eff}} = 1/2$ state, the observed uniform magnetic moment $0.07 \mu_B/\text{Ir}$ indicates the canted angle $\sim 4^\circ$. This is much smaller than $\alpha \sim 23^\circ$. The reason for this discrepancy between the theory and experiment is likely related to a reduced spin moment due to quantum fluctuations, a slight deviation from the $J_{\text{eff}} = 1/2$ state, or the effect of the direct interaction which is not considered in the present analysis.

To summarize, we have investigated the spin and orbital state of CaIrO_3 post-perovskite by the resonant x-

ray diffraction. The orbital of a t_{2g} hole is the $J_{\text{eff}} = 1/2$ state. This strongly spin-orbit coupled state stabilizes a striped-type magnetic order. We also propose the anisotropic tensor of susceptibility scattering as a tool to investigate the orbital character in a metallic iridate.

We thank Y. Ueda for the use of a single crystalline x-ray diffractometer. The synchrotron radiation experiments were performed at BL19LXU and BL02B1 in SPring-8 with the approval of RIKEN (Proposal No. 20090064) and the Japan Synchrotron Radiation Research Institute (JASRI) (Proposal No. 2009B1200), respectively. This work was supported by Special Coordination Funds for Promoting Science and Technology, Promotion of Environmental Improvement for Independence of Young Researchers, and Grant-in-Aid for Scientific Research (B) (No. 20740211).

-
- [1] B. J. Kim, Hosub Jin, S. J. Moon, J.-Y. Kim, B.-G. Park, C. S. Leem, Jaejun Yu, T. W. Noh, C. Kim, S.-J. Oh, J.-H. Park, V. Durairaj, G. Cao, and E. Rotenberg, *Phys. Rev. Lett.* **101**, 076402 (2008).
 - [2] B. J. Kim, H. Ohsumi, T. Komesu, S. Sakai, T. Morita, H. Takagi, and T. Arima, *Science* **323**, 1329 (2009).
 - [3] D. Pesin and L. Balents, *Nat. Phys.* **6**, 376 (2010).
 - [4] B.-J. Yang and Y. B. Kim, *Phys. Rev. B* **82**, 085111 (2010).
 - [5] H. Watanabe, T. Shirakawa, and S. Yunoki, *Phys. Rev. Lett.* **105**, 216410 (2010).
 - [6] G. Jackeli and G. Khaliullin, *Phys. Rev. Lett.* **102**, 017205 (2009).
 - [7] S. Hirai, M. D. Welch, F. Aguado, S. A. T. Redfern, *Z. Kristallogr.* **224** 345 (2009).
 - [8] K. Ohgushi, H. Gotou, T. Yagi, Y. Kiuchi, F. Sakai, and Y. Ueda, *Phys. Rev. B* **74**, 241104 (2006).
 - [9] M. Blume, *J. Appl. Phys.* **57**, 3615 (1985).
 - [10] D. F. McMorrow, S. E. Nagler, and K. A. McEwen, and S. D. Brown, *J. Phys. Condens. Matter.* **15**, L59 (2003).
 - [11] X. Liu, T. Berlijn, W.-G. Yin, W. Ku, A. Tsvelik, Young-June Kim, H. Gretarsson, Yogesh Singh, P. Gegenwart, and J. P. Hill, *Phys. Rev. B* **83**, 220403(R) (2011).
 - [12] K. Ishii, I. Jarrige, M. Yoshida, K. Ikeuchi, J. Mizuki, K. Ohashi, T. Takayama, J. Matsuno, and H. Takagi, *Phys. Rev. B* **83**, 115121 (2011).
 - [13] See supplementary material for specific details of the data analysis and calculation.
 - [14] M. Yabashi, T. Mochizuki, H. Yamazaki, S. Goto, H. Ohashi, K. Takeshita, T. Ohata, T. Matsushita, K. Tamasaku, Y. Tanaka, and T. Ishikawa, *Nucl. Instr. Meth. Phys. Res. A* **467-468**, 678 (2001).
 - [15] K. Sugimoto, H. Ohsumi, S. Aoyagi, E. Nishibori, C. Moriyoshi, Y. Kuroiwa, H. Sawa, and M. Takata, *AIP Conf. Proc.* **1234**, 887 (2010).
 - [16] The magnetic reflection can be written as $I_{\text{mag}} \propto |\sum_j \hat{\mathbf{R}}\mathbf{S}_j \cdot \boldsymbol{\epsilon}_i \times \boldsymbol{\epsilon}_s e^{2\pi i \mathbf{q} \cdot \mathbf{r}_j}|^2$, where \mathbf{q} is the momentum transfer and \mathbf{r}_j is the position of the j -th Ir atom.
 - [17] We can phenomenologically deduce the tensor structure amplitude for the ATS scattering following V. E. Dmitrienko, *Acta Cryst.* **A39**, 29 (1983). The result ac-

cords with our microscopic calculation.

- [18] I. Zegkinoglou, J. Stremper, C. S. Nelson, J. P. Hill, J. Chakhalian, C. Bernhard, J. C. Lang, G. Srajer, H. Fukazawa, S. Nakatsuji, Y. Maeno, and B. Keimer, Phys. Rev. Lett. **95**, 136401 (2005).
- [19] S. J. Moon, H. Jin, K. W. Kim, W. S. Choi, Y. S. Lee, J. Yu, G. Cao, A. Sumi, H. Funakubo, C. Bernhard, and T. W. Noh, Phys. Rev. Lett. **101**, 226402 (2008).
- [20] O. B. Korneta, Tongfei Qi, S. Chikara, S. Parkin, L. E. De Long, P. Schlottmann, and G. Cao, Phys. Rev. B **82**, 115117 (2010).
- [21] F. Wang and T. Senthil, Phys. Rev. Lett. **106**, 136402 (2011).